Convectively Driven Mesoscale Weather Systems Aloft. Part II: Numerical Simulations

J. M. FRITSCH AND R. A. MADDOX

NOAA, Environmental Research Laboratories, Office of Weather Research and Modification, Boulder, CO 80303

(Manuscript received 24 April 1980, in final form 11 October 1980)

ABSTRACT

A fine-mesh, 20-level, primitive equation model is used to study the generation of convectively driven weather systems in the vicinity of the tropopause. In a test simulation, a high-level (~200 mb) mesoscale high pressure system forms in conjunction with the development of a convective complex. In response to this high-level mesohigh, winds aloft rapidly decelerate as they approach the convective complex. On the other hand, downstream of the convective system the mesoscale pressure gradient accelerates the wind to generate a jet maximum which is stronger than any wind speed prior to the development of the convection.

The formation of the high-level mesohigh appears to be linked to the convectively forced production of a layer of cold air above the tropopause. The cold layer of air is generated by cloud-scale cooling from overshooting tops and from adiabatic cooling by strong (~0.5 m s^{-1}) mesoscale lifting in response to the convective cloud warming below the tropopause.

The model-generated high-level convective system is compared to observed systems and briefly discussed in light of the interaction of these systems with their larger scale environment.

1. Introduction

Until recently, the problem of predicting convective clouds and their attendant weather phenomena has often been perceived as predicting loosely organized, subgrid-scale processes. Studies by Ninomiya (1971), Maddox (1980a,b) and Fritsch and Maddox (1981), however, have shown that convective processes during the warm season in the United States often are not subgrid scale. Rather, convective systems exhibit a high degree of organization and significantly impact their larger scale environment. In addition to the mesohighs and lows that routinely appear in the boundary layer (see, e.g., Fig. 1 and Magor, 1959) convective systems also impose intense meso-α scale[1] anticyclonic perturbations on the mean flow at tropopause levels. Fig. 2 shows an infrared satellite image of a mesoscale convective complex with the vector wind errors of the 12 h LFM predicted 200 mb wind field superimposed. A composite of 10 such events is shown in Fritsch and Maddox (1981). As in the Fig. 2 example, the composite analysis also shows a well-defined meso-α scale anticyclonic perturbation with vector wind errors as large as 24 m s^{-1}. The strong organization of the convection suggests a much greater potential for successful prediction than heretofore considered possible.

One of the major difficulties in developing a predictive capability for these systems [now termed Mesoscale Convective Complexes—MCC's after Maddox (1980b)] is that we do not yet possess the physical understanding of how the organization takes place. This paper presents the results of preliminary numerical studies to understand the processes and circulations responsible for the development of such deep, mesoscale convective systems. Section 2 contains a brief summary of the mesoscale numerical model while in Section 3 results of simulating a small (~200 km) convective complex are presented. Sections 3 and 4 consider the mesoscale structure generated by the model and its implications for future modeling and prediction.

2. Mesoscale numerical model

The primary model characteristics and convective parameterization assumptions are listed below. A complete description is available in Fritsch and Chappell (1980a,b).

a. Numerical model characteristics

1) The conservation of momentum equations are cast in the primitive equation flux form.

2) Height is the vertical coordinate with 20 constant height levels defined at the climatological mean heights of significant pressure levels (i.e., every 50 mb).

3) The horizontal domain is 400 km on a side with

[1] Meso-α scale is defined here as 250–2500 km.

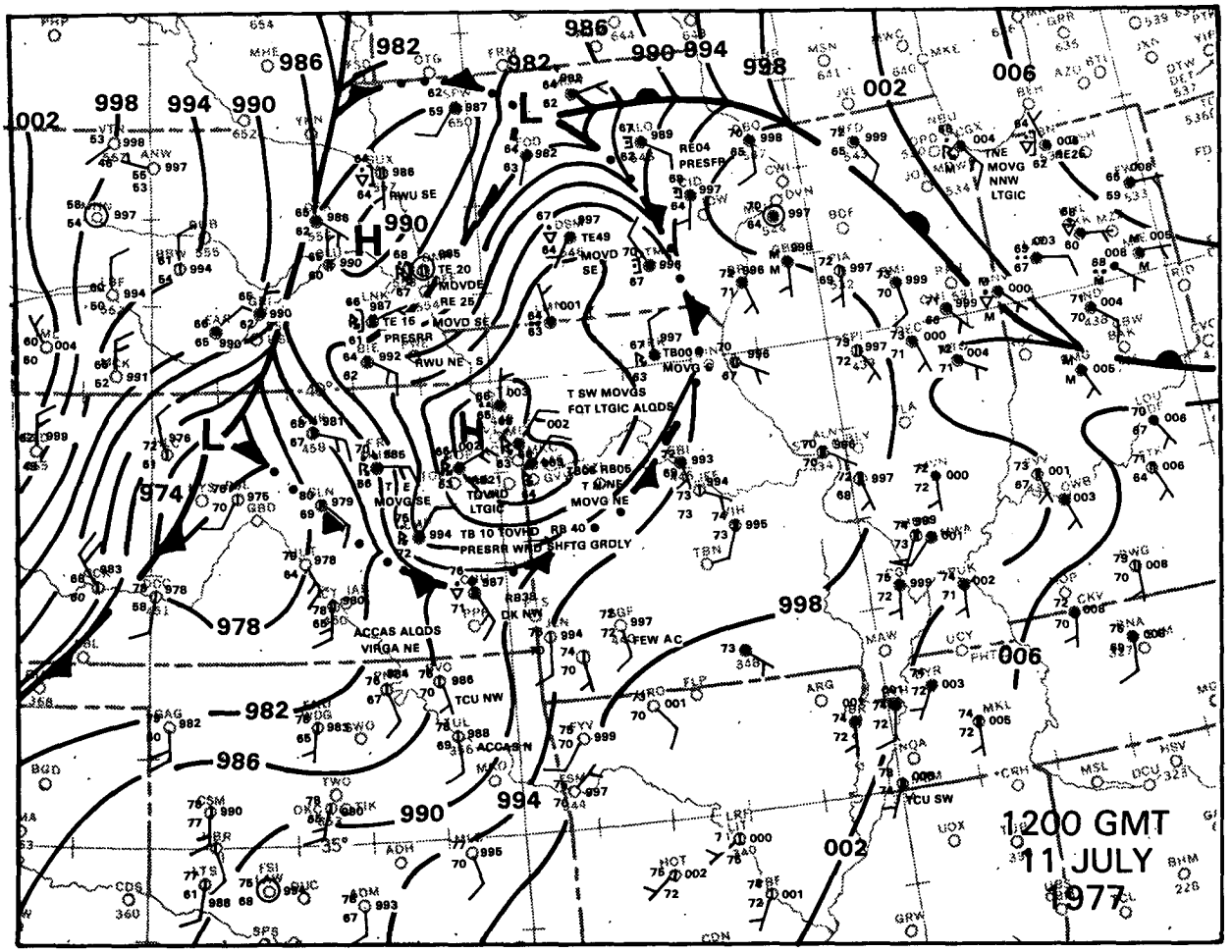

FIG. 1. Surface mesoanalysis for 1200 GMT 11 July 1977.

a 20 km grid mesh. Both the domain and mesh are arbitrary.

4) Detailed surface topography is not included.

5) Lateral boundaries are periodic at the east and west and constant at the north and south. A "sponge" condition is applied to the prognostic tendencies along the north and south boundaries.

6) The upper boundary condition requires the vertical motion to be zero or $dz/dt = w = 0$.

7) The lower boundary condition includes a surface drag with linear drag decrease through the transition layer. Also, $w = 0$.

8) The finite-difference formulations are centered in time and space, and a time filter is included to avoid separation of solutions. Time steps are 30 s.

9) A horizontal diffusion filter, applied as a smoother-desmoother, is used to help control numerical and boundary-generated noise.

10) Vertical temperature and density adjustments have been neglected except in the moist convective calculations.

11) The governing system of equations is hydrostatic with non-hydrostatic effects included through the convective parameterization. Pressure, u and v components of the wind, and mixing ratio are the prognostic variables while temperature is diagnosed hydrostatically, and density is derived using the gas law. Vertical motion is diagnosed using Richardson's equation.

b. Convective parameterization assumptions and constraints

1) Moist convection only occurs when air is forced to its level of free convection (i.e., when potential buoyant energy becomes available).

2) Mass transports by moist convection are closely approximated by a model cloud ensemble which treats *deep* convection as the dominant cloud form.

3) Precipitation efficiency of the convective clouds is inversely proportional to the vertical wind shear across the cloud depth.

4) The grid-scale stabilization rate (destruction of Available Buoyant Energy, ABE) by moist convec-

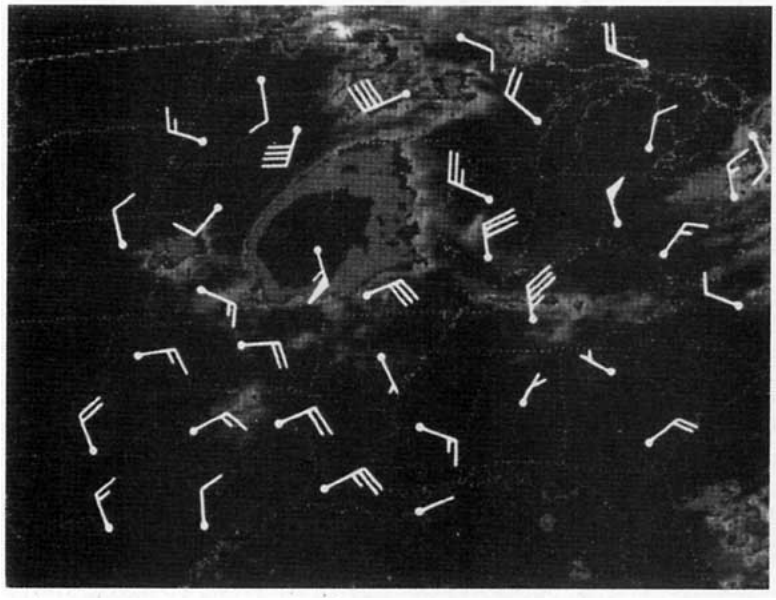

FIG. 2. Infrared satellite imagery of mesoscale convective complex at 1200 GMT 28 June 1979. Wind barbs are vector errors of the 12 h LFM predicted 200 mb wind field. Full wind barb = 5 m s^{-1}; flag = 25 m s^{-1}.

tive processes is equivalent to minus the model-generated ABE divided by the estimated time for the convective "cells" to move across the grid element. This time period τ_c is obtained by dividing the grid length by the mean environmental wind speed over the cloud depth; τ_c has a lower limit defined by the average lifetime of individual cells (30 min), and an upper limit (1 h) to allow large-scale changes to alter the characteristics of the convective clouds. If the period of time necessary to consume all of the ABE is >1 h, the computed rate of stabilization is still applied for 1 h, even though all the ABE will not be consumed. After an hour the atmosphere is again checked for instability and convection may be initiated once again (at different adjustment rates, however).

5) The vertical distribution of the convective heating and cooling of environmental air is the resultant structure that occurs when (i) the cloud model processes sufficient mass to produce the net stabilization by moist convection as specified in (4)

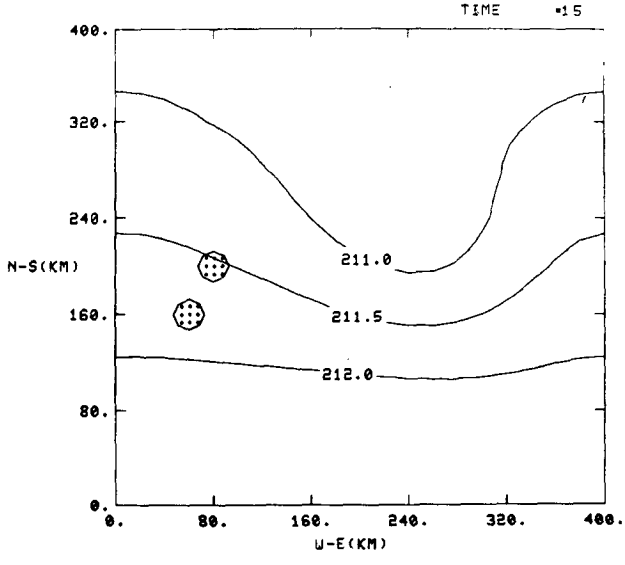

FIG. 3. Pressure (mb) at 11.8 km level and area of active convection (shaded) 15 min after convection began.

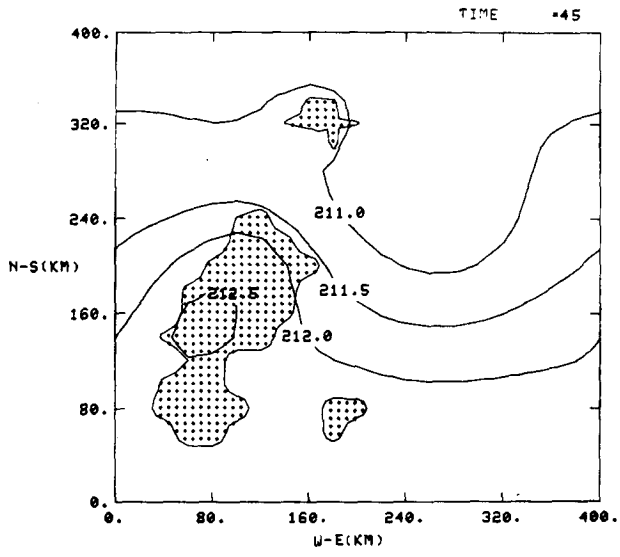

FIG. 4. As in Fig. 3 except 45 min after convection began.

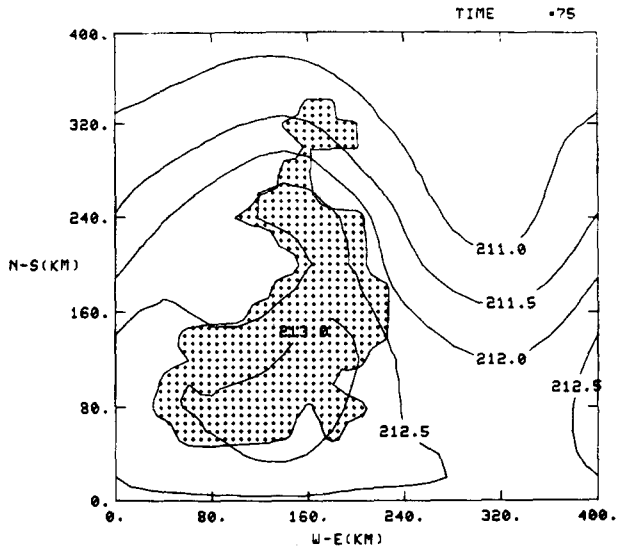

FIG. 5. As in Fig. 3 except 75 min after convection began.

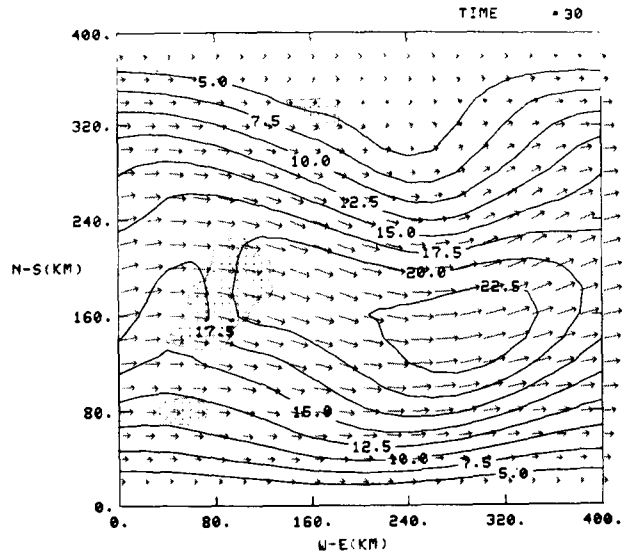

FIG. 7. Isotachs (m s^{-1}, solid lines), wind direction (arrows) and location of active convection (shaded) at 11.8 km level 30 min after convection began.

above; and (ii) the environmental vertical motion field adjusts to the mass requirements of the convective cloud model and the larger scale vertical transports.

6) The changes in temperature and mixing ratio at a model grid point are the sum of the effects of compensating subsidence in the environment plus the effect of area-weighting the cloud updraft, downdraft and environment.

7) Momentum is vertically exchanged through bulk mixing processes in the cloud updrafts and downdrafts and by compensating environmental vertical motions.

The effects of the convective processes on the mesoscale are gradually fed into the governing system of equations. Changes are linearly introduced over the period of time defined by τ_c. Temperature changes are incorporated into the governing system through heating terms which appear in the pressure tendency and vertical motion equations.

3. Initial conditions and results

Initial conditions were analytically generated to simulate a situation conducive to development of a

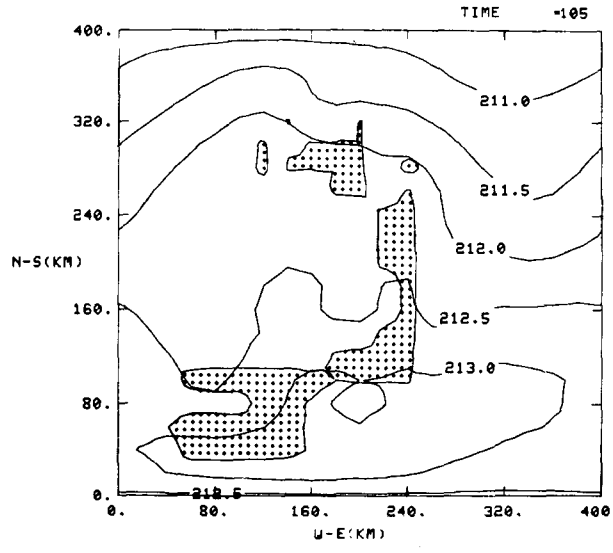

FIG. 6. As in Fig. 3 except 105 min after convection began.

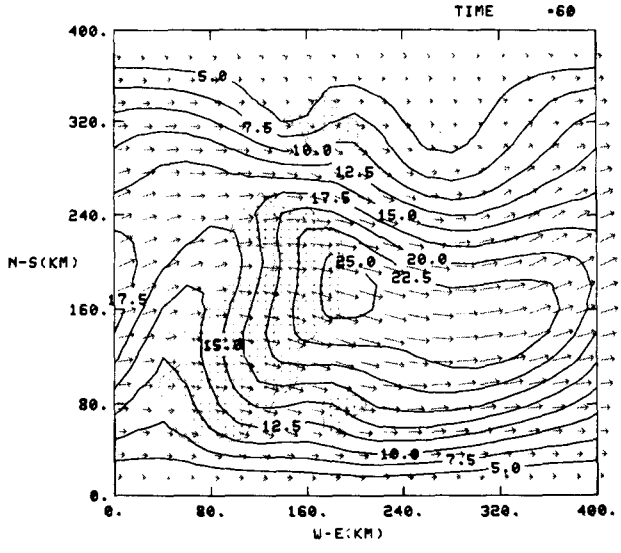

FIG. 8. As in Fig. 7 except for 60 min after convection began.

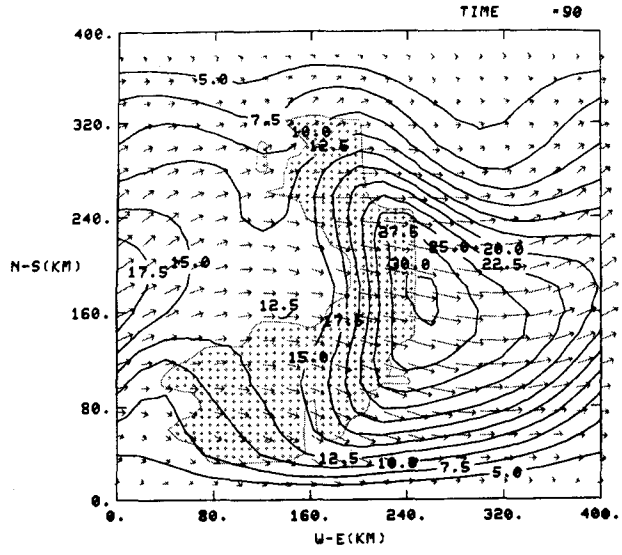

FIG. 9. As in Fig. 7 except for 90 min after convection began.

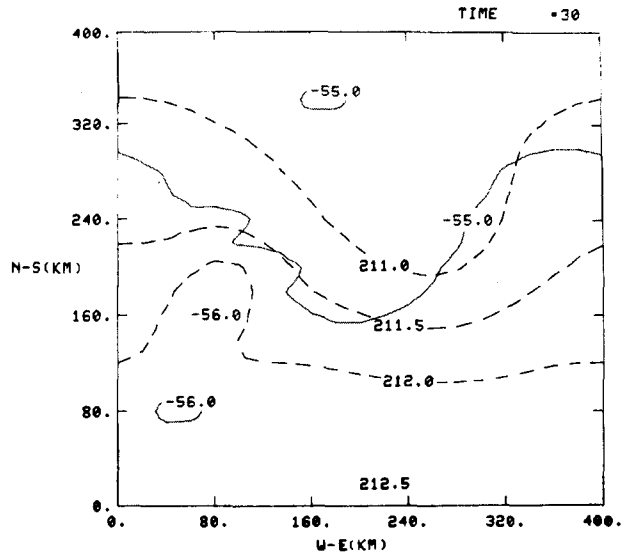

FIG. 11. Pressure (mb, dashed lines) at 11.8 km level and temperature (°C, solid lines) at 13.6 km level for 30 min after convection began.

convective complex (Fritsch *et al.*, 1980). These conditions were designed to simulate a "short" (mesoscale) wave propagating through a slower moving synoptic-scale wave. The area of upward motion traveling with the short wave encounters a narrow moist tongue in the synoptic-scale warm sector and, along with the boundary-layer warming, initiates deep convection.

Figs. 3–6 show the numerical model evolution of convection and the corresponding pressure pattern at 11.8 km (~200 mb level). Immediately following the convective outbreak, pressure begins to rise along the axis of the convection and forms a mesoscale ridge aloft. The ridge moves eastward with the convection, producing a continuous acceleration of the wind immediately downstream of the convective line. The changing isotach and wind direction patterns at 11.8 km are shown in Figs. 7–10. After one hour of convection, a distinct wind speed maximum, larger than any wind speed prior to convection, has formed downwind of the convective complex. This jet maximum continues to increase in strength until the central portion of the convective line dissipates. The magnitude of the jet maximum then diminishes.

Formation of the ridge aloft seems to be correlated

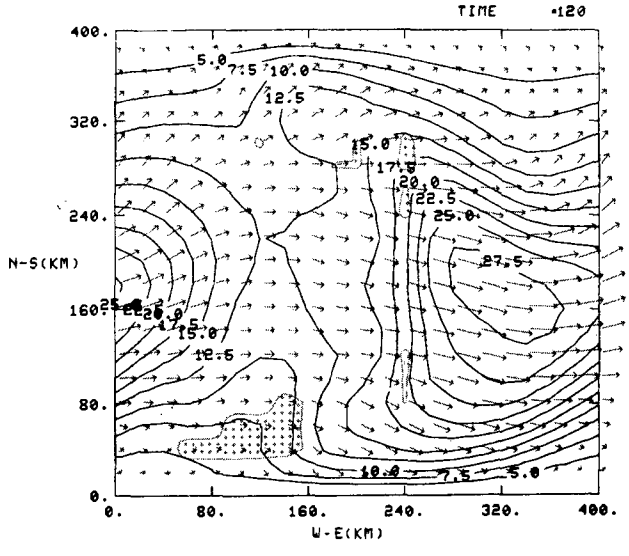

FIG. 10. As in Fig. 7 except for 120 min after convection began.

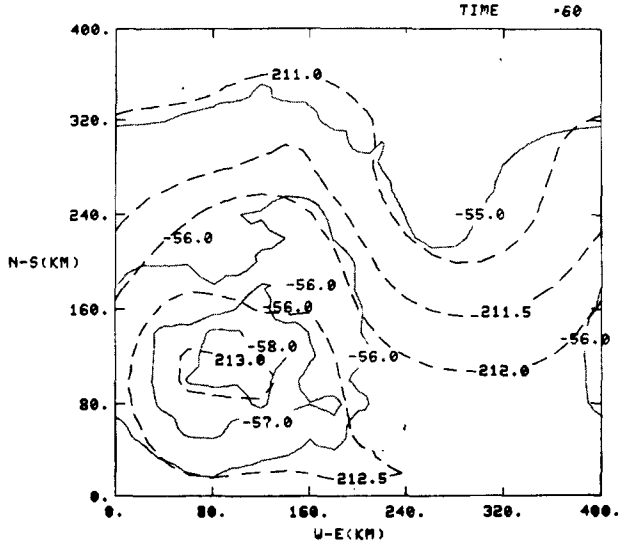

FIG. 12. As in Fig. 11 except for 60 min after convection began.

with cooling in the lower stratosphere. Figs. 11 and 12 show the evolution of the temperature field at the 13.6 km level (~150 mb) superimposed on the pressure field at the 11.8 km level. Note that the mesohigh is centered beneath the core of the cold pool. This high-level pool of cold air was generated by two separate processes. First, strong cooling occurred with the outflow from overshooting cloud tops. Fig. 13 shows a vertical cross section of convective cloud heating of the environment 45 min after convection began. Note that in addition to the cooling in the lower stratosphere, strong warming is occurring in the upper troposphere (~10–14 km). As pointed out by Anthes and Keyser (1979), the environment is very sensitive to the vertical distribution of convective heating. In this particular case, the tropospheric warming induces a mesoscale upward circulation across the region of active convection (see Fig. 14). This mesoscale circulation also is seen in the vertical cross section (Fig. 15) passing (east–west) through the center of the high-level cold pool. Figs. 14 and 15 show that the mesoscale circulation extends through the 13.6 km level. Thus, in addition to the direct cooling by the overshooting deep convective clouds, the lower stratosphere may also be cooled by adiabatic expansion on the ascending branch of the mesoscale circulation. Aside from these modeling results, other evidence for *mesoscale* ascent comes from several disparate sources. Specifically, Fankhauser (1969, 1974), Sanders and Emanuel (1977) and Ogura and Chen (1977) have diagnosed such a circulation for squall lines passing through the National Severe Storms Laboratory's upper air sounding network

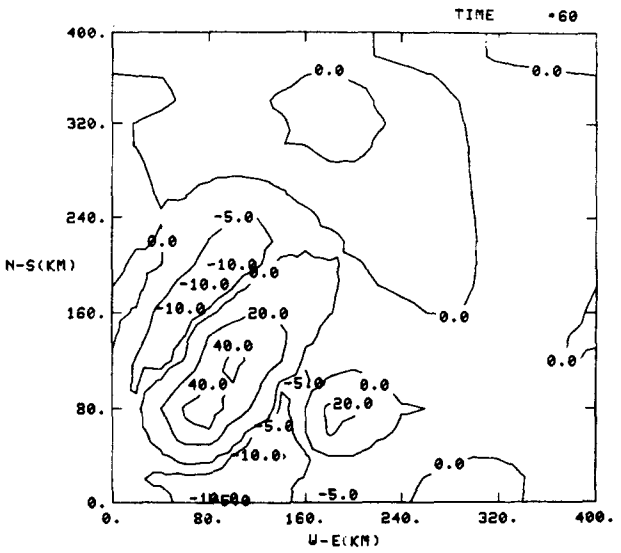

FIG. 14. Vertical motion (cm s^{-1}) at 13.6 km level (~150 mb).

in Oklahoma. Broad areas of steady rain, persisting for several hours, frequently develop following the maturation of large convective complexes [note steady rain area in Fig. 1; also see Maddox (1980b), Houze (1977), Zipser (1977) and Leary and Houze (1979)]. Finally, Kreitzberg and Perkey (1977) and Brown (1979) found mesoscale vertical circulations developed in response to the convection in their mesoscale numerical models.

The exact role of such a circulation in the development of mesoscale weather systems is unclear at this time. However, this type of circulation may be a mechanism by which convection interacts "up-

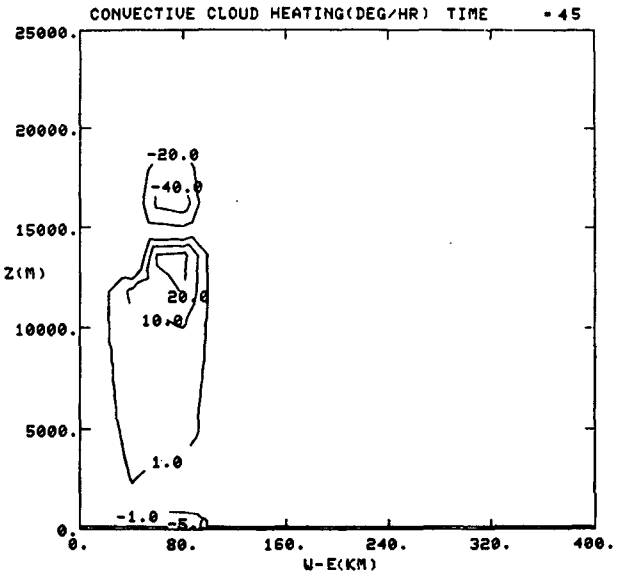

FIG. 13. Vertical cross section of convective cloud heating of the environment. Section passes east–west and was taken 100 km north of origin (see Fig. 14).

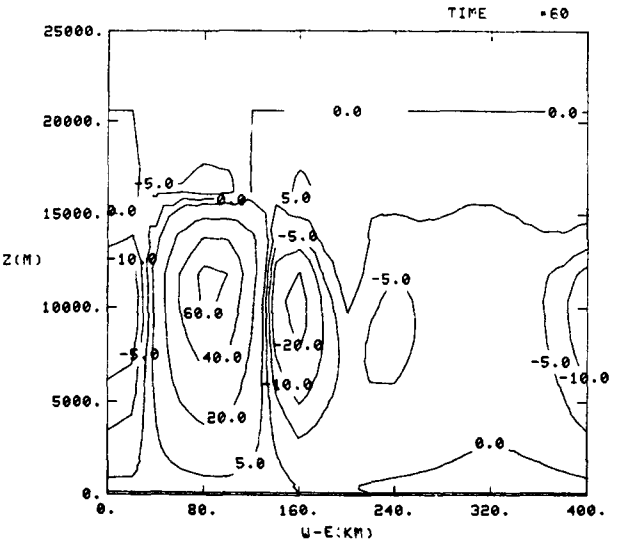

FIG. 15. Vertical cross section of vertical motion (cm s^{-1}). Section passes east–west and was taken 100 km north of origin (see Fig. 14).

scale" with its environment to organize and enhance future convective growth. To this end, Hoxit *et al.* (1976) and Fritsch and Chappell (1980b) argued that the subsidence portion of this circulation was responsible for hydrostatic production of surface mesotroughs and mesolows.

Clearly, at this juncture, one must keep in mind that, at least for the numerical model, the mesoscale response to convection is strongly dependent on initial conditions and how the convective parameterization introduces the convective heating and cooling.

4. Summary and discussion

Comparison of the modelling results to the observed convective systems described by Fritsch and Maddox (1981) suggests that some of the proper physics for generating convectively driven mesoscale weather systems are being introduced into the mesoscale model through the convective parameterization. The development of a region of mean mesoscale ascent is particularly important since it is a strong indication of "upscale" organization by the convection. Maddox (1980a,b) and Fritsch and Maddox (1981) further discuss the significance of this circulation.

Although the model reproduces some of the observed characteristics of high-level mesosystems, the mesohigh and associated wind perturbation produced in the simulation are relatively small and short-lived compared to the systems being studied by Maddox (1980a,b) and Fritsch and Maddox (1981). On these small time and space scales, the Coriolis force does not act long enough nor over a large enough area to be able to produce a large anticyclonic perturbation. Further modelling studies using larger domains and longer time periods are required to simulate the type of anticyclonic structures being forced by the meso-α scale convective complexes. Although the model results offer some support for the supposition that the mean upward circulation developing in response to the deep convection is responsible (at least in part) for the high-level anticyclogenesis, firm understanding remains elusive.

Acknowledgments. The authors gratefully acknowledge the support of Drs. C. F. Chappell and E. C. Nickerson. The manuscript was skillfully prepared by Mrs. Elaine Ardourel.

This work was partially supported by the Water and Power Resources Service, Office of Atmospheric Resources Management.

REFERENCES

Anthes, R. A., and D. Keyser, 1979: Tests of a fine-mesh model over Europe and the United States. *Mon. Wea. Rev.*, **107,** 963–984.

Brown, J. M., 1979: Mesoscale unsaturated downdrafts driven by rainfall evaporation: A numerical study. *J. Atmos. Sci.*, **36,** 313–338.

Fankhauser, J. C., 1969: Convective processes resolved by a mesoscale rawinsonde network. *J. Appl. Meteor.*, **8,** 778–798.

——, 1974: The derivation of consistent fields of wind and geopotential height from mesoscale rawinsonde data. *J. Appl. Meteor.*, **13,** 637–646.

Fritsch, J. M., and C. F. Chappell, 1980a: Numerical prediction of convectively driven mesoscale pressure systems. Part I: Convective parameterization. *J. Atmos. Sci.*, **37,** 1722–1733.

——, and ——, 1980b: Numerical prediction of convectively driven mesoscale pressure systems. Part II: Mesoscale model. *J. Atmos. Sci.*, **37,** 1734–1762.

——, and R. A. Maddox, 1981: Convectively driven mesoscale weather systems aloft. Part I: Observations. *J. Appl. Meteor.*, **20,** $$$–$$$.

——, E. L. Magaziner and C. F. Chappell, 1980: Analytical initialization for three-dimensional numerical models. *J. Appl. Meteor.*, **19,** 809–818.

Houze, R. A., 1977: Structure and dynamics of a tropical squall-line system. *Mon. Wea. Rev.*, **105,** 1540–1567.

Hoxit, L. R., C. F. Chappell and J. M. Fritsch, 1976: Formation of mesolows and pressure troughs in advance of cumulonimbus clouds. *Mon. Wea. Rev.*, **104,** 1419–1428.

Kreitzberg, C. W., and D. J. Perkey, 1977: Release of potential instability: Part II. The mechanism of convective-mesoscale interaction. *J. Atmos. Sci.*, **34,** 1569–1595.

Leary, C. A., and R. A. Houze, Jr., 1979: The structure and evolution of convection in a tropical cloud cluster. *J. Atmos. Sci.*, **36,** 437–457.

Maddox, R. A., 1980a: An objective technique for separating macroscale and mesoscale features in meteorological data. *Mon. Wea. Rev.*, **108,** 1108–1121.

——, 1980b: Mesoscale convective complexes. *Bull. Amer. Meteor. Soc.*, **61,** 1374–1387.

Magor, B. W., 1959: Mesoanalysis: Some operational techniques utilized in tornado forecasting. *Bull. Amer. Meteor. Soc.*, **40,** 499–511.

Ninomiya, K., 1971: Mesoscale modification of synoptic situations from thunderstorm development as revealed by ATS III and aerological data. *J. Appl. Meteor.*, **10,** 1103–1121.

Ogura, Y., and Y. Chen, 1977: A life history of an intense mesoscale convective storm in Oklahoma. *J. Atmos. Sci.*, **34,** 1458–1476.

Sanders, F., and K. A. Emanuel, 1977: The momentum budget and temporal evolution of a mesoscale convective system. *J. Atmos. Sci.*, **34,** 322–330.

Zipser, E. J., 1977: Mesoscale and convective-scale downdrafts as distinct components of squall-line structure. *Mon. Wea. Rev.*, **105,** 1568–1589.